A coarse-grained model for polyethylene glycol in bulk water and at a water/air interface

Khongvit Prasitnok[a,b] **and Mark R. Wilson,**[*a]

Received Xth XXXXXXXXXX 20XX, Accepted Xth XXXXXXXXX 20XX
First published on the web Xth XXXXXXXXXX 200X
DOI: 10.1039/b000000x

A coarse-grained model for polyethylene glycol (PEG) in water has been developed using a combination of the iterative Boltzmann inversion (IBI) methodology and a suitable coarse-grained water potential. The combined coarse-grained model is shown to be effective in reproducing the properties of single chains in bulk water and multiple chains across a series of chain lengths and concentrations, and is transferable to PEG chains at a water/air interface. Good agreement is achieved with both experiment and reference atomistic simulations in an explicit solvent. Simulations of a single chain in aqueous solution yield a molecular weight (M_W)-radius of gyration (R_g) relation that compares favourably with the reported scaling law from experiment. Simulations of multiple chains across a wide concentration range show no concentration dependence of R_g, in agreement with previous atomistic simulations. The model we develop is shown to be transferable between polymer in bulk water and at a water/air interface. For interfacial simulations, PEG chains are found to spontaneously migrate to the surface and adsorb to form a thin surface layer, which thickens with increasing surface concentration. The point at which the surface is fully saturated with polymer, and the polymer layer thicknesses obtained from simulations, are both in good agreement with experimental findings. At high surface concentrations, when the surface is fully saturated with polymer, ethylene oxide (EO) segments are found to extend into the water subphase as loop and tail conformations, with this extension increasing with further increases in the surface concentration. The coarse-grained model is noted to provide very large increases in simulation speed, with equilibration times of $< 1000\times$ the reference atomistic models. We also consider a number of different coarse-grained models for water in this study, showing that the CSJ model adopted in this work [Chiu et al., J. Chem. Theory Comput. 2010, **6**, 851] is far superior for studying water at a water/air surface, than many of the previous coarse-grained models of water.

1 Introduction

Polyethylene glycol (PEG) (often known as poly(oxyethylene), POE, poly(ethylene oxide) or PEO in its longer chain form) is one of the best known water soluble polymers. Interest in PEG/PEO arises from the fascinating behaviour of ethylene oxide chains in aqueous solutions[1–3], as well as the ability of chains to adsorb on surfaces and at interfaces, leading to a wide variety of applications[4]. Long ethylene oxide chains are known to exhibit a closed-loop region of immiscibility in the polymer/water phase diagram, which is dependent on chain length[1]. The properties of short oligomers are subtly influenced by both chain length and by end substitution. PEG, in pure form, is terminated by hydroxyl groups (H-[O-CH_2-CH_2]$_n$-O-H), whereas the common dimethyl ether form (CH_3-[O-CH_2-CH_2]$_n$-O-CH_3) is slightly more hydrophobic. There has been considerable interest in understanding the properties of ethylene oxide chains in water, not least because of their ubiquitous use as nonionic surfactants when coupled to hydrophobic moieties[5], and their medical use when covalently coupled to proteins or drug molecules by the process of PEGylation[6].

Alongside experimental studies of the solubility and adsorption of PEG/PEO, it is highly desirable to obtain a molecular understanding of the behaviour of these polymers using computational models. Despite recent improvements in computer power, which allow for the simulation of many soft matter systems at full atomistic detail[7–10], it is still impractical to use this technique to study large and/or slowly relaxing systems. This is especially true in the area of polymers where, for moderate chain lengths, relaxation times can easily extend beyond hundreds of nanoseconds. To overcome the limited time and length scales accessible to atomistic models, a range of successful coarse-grained (CG) molecular models have been introduced[11–18]. Usually, CG models provide a considerable speed-up in terms of computer time compared to their atomistic counter parts. Increases in speed arise from three factors: simply reducing the number of interaction sites in comparison to atomistic models, increasing the time step used (in the case of dynamics simulations) facilitated by softer interaction po-

[a] *Department of Chemistry, Durham University, South Road, Durham, DH1 3LE, United Kingdom. E-mail: mark.wilson@durham.ac.uk*
[b] *Department of Chemistry, Faculty of Science, Mahasarakham University, Maha Sarakham 44150, Thailand.*
∗ *Author for correspondence.*

tentials, and quicker movement of the system through configurational space due to smaller energy barriers and/or a smoother energy landscapes.

Various coarse-grained models for PEG/PEO and PEG-related systems have been developed recently. For bulk PEG, Wang et al.[19] have implemented coarse-grained models based on two schemes: an inversion procedure from reference nonbonded pair correlation functions obtained by atomistic simulation, which yields coarse-grained potentials from the Ornstein-Zernike equation with a Percus-Yevick closure relation (OZPY^{-1}); and a OZPY^{-1}scheme with further refinement involving iterative Boltzmann inversion (IBI)[20,21]. They successfully use a series of $C_4H_8O_2$ beads (a mapping of 2 monomers to 1 bead) to represent the polymer ignoring complications from end termination groups. For a degree of polymerization of 20, they showed good agreement between atomistic and coarse-grained models for structural properties of PEG, and the model proved to be transferable to a longer 40 EO monomer chain. Chen et al.[22] have used a similar degree of coarse-graining in their model for bulk PEG, working with ethyl terminated chains. Fitting to atomistic reference simulations, they used a 8:6 Lennard-Jones potential for nonbonded interactions, together with IBI derived intramolecular potentials for 27 ethyl-[O-CH_2-CH_2]$_{30}$ chains, and show good agreement with static structure factors from neutron diffraction. For polymer in water, Fischer and coworkers have extensively investigated a solvent-less (i.e. implicit solvent) model for dimethyl terminated EO chains[23] obtained via IBI with each monomer mapped to a single CG bead. Their model was found to yield good results for PEO structures in comparison to atomistic simulations and experiments. They also extensively tested the transferability of their model and the differences induced by mapping from a 3-monomer and a 10-monomer atomistic reference model. Transferability was found to be very good across a wide concentration range. Lee et al.[24] have extended the MARTINI CG force field[16] to PEG systems in water. Within the MARTINI scheme, CG beads are mapped to 3 or 4 extended atoms using a 12:6 Lennard-Jones potential and a single "water bead" represents 4 water molecules. For PEG/PEO a single C_2H_4O bead unit can be used to represent the relevant atoms. Hence, hydroxyl-terminated PEG polymers of the form H-[O-CH_2-CH_2]$_n$-O-H, are represented by n beads (subsuming the terminal OH), and methyl terminated chains, CH_3-[O-CH_2-CH_2]$_n$-O-CH_3 (termed PEO in MARTINI) can be mapped directly onto $n+1$ beads (subsuming the terminal Hs). Despite the relative steepness of the $1/r^{12}$ short range repulsive potential in MARTINI (in comparison to other CG PEG models), the potentials developed were found to be transferable between systems of pure low-molecular weight methyl-terminated chains and also chains in dilute aqueous solution, with good agreement shown between simulated and experimentally observed quantities[24]. A new MARTINI CG PEG model, suitable for the longer molecular dynamics time steps typically used with MARTINI, has recently been developed and validated against radius of gyration data from atomistic simulations and experiment[25]. Several PEG/PEO potentials have also been employed successfully within model amphiphilic systems, including an implicit solvent model by Bedrov et al.[26] with a single monomer mapped to each coarse-grained bead, used to study the formation of micelles from a poly(ethylene oxide)-poly(propylene oxide)-poly(ethylene oxide) triblock copolymer in aqueous solution, and the models of Klein and coworkers[27,28] which perform well in terms of reproducing self-assembly of PEO surfactants.

An inherent weakness of coarse-grained modelling arises from potentials which tend to be state point dependent, with the balance of entropic and enthalpic effects often being shifted in the act of coarse-graining. However, the extent to which models can be used outside their parametrization range varies dramatically between different CG approaches. In the current work, we wanted to develop a coarse-grained model that was suitable for studying poly(ethylene glycol)dimethylether (PEG-DME), CH_3-[O-CH_2-CH_2]$_n$-O-CH_3, chains in both aqueous solution and at a water/air interface. Our initial tests of several existing CG potentials immediately caused problems, either through issues with water models required for building a water/air interface (the surface tension of many CG models is very low - such that they can not support a water/air interface at all) or problems with the transferability of EO potentials. However, we show in the current work that the combination of a suitable analytical water potential, due to Chiu et al.[29], combined with an iterative Boltzmann approach (as used successfully in the implicit solvent models of Chen et al.[22] and Fischer et al.[23]) can be used to produce an extremely efficient computational model suitable to study both the conformational behaviour of this polymer in aqueous solution and its behaviour at a water/air interface.

The structure of the paper is as follows: in section 2 we describe the reference atomistic simulations used and the coarse-grained simulation approach; in section 3 we describe the testing of a series of coarse-grained water models for suitability and discuss the results for the coarse-grained PEG/water model developed here; we draw conclusions and summarize in section 4.

2 Computational details

2.1 Atomistic simulations

Atomistic reference systems were used for fitting the coarse-grained potentials developed in this work. The atomistic reference simulations used molecular dynamics performed with the GROMACS 4.0.7 package[30]. A modified TraPPE-UA force

field[31] was used for the PEG-DME model and the TIP4P-Ew potential[32] was used for water. The modified TraPPE-UA force field originated from the TraPPE-UA force field by Siepmann et al. [33], with dihedral parameters later parametrised to match *ab initio* data by Anderson and Wilson[34] to improve the conformer equilibria. This modified force field in combination with the TIP4P-Ew water model provides a good description of PEG oligomers in aqueous solution. The equations of motion were integrated using the leap-frog algorithm[35] with a time step of 2 fs. The temperature was kept constant at 298 K by using a Nosé-Hoover thermostat[36,37] with a relaxation time of 2.5 ps. A Rahman-Parrinello barostat[38] with relaxation time of 5 ps was employed when constant pressure simulations were needed. Electrostatic interactions were calculated using particle mesh Ewald[39] with a real space cutoff of 9 Å. Lennard-Jones interactions were truncated at 9 Å, with long-range corrections for both potential and pressure applied. Neighbour lists were updated every 10 time steps using a list cutoff radius of 9 Å. Here, periodic boundary conditions have been applied for all simulations. Bond constraints were solved using the Linear Constraint Solver (LINCS) algorithm[40] with a linc-order of 4 (number of matrices in the matrix inversion).

The atomistic reference system (used for the coarse-graining process) was constructed as follows. A CH_3-(O-CH_2-CH_2)$_9$-O-CH_3 (PEG10) chain was assembled and subjected to stochastic dynamics simulations in order to allow an initially linear chain to collapse into a more realistic random coil arrangement. The aqueous simulation was set by placing 16 relaxed PEG10 chains into a 50.0 Å/side box of 1600 water molecules. This initial system was subjected to a short *NpT* equilibration run to allow the density of the system to reach equilibrium. This resulted in the system box size decreasing to 38.9 Å for all dimensions. Reported results were then evaluated from constant-*NVT* production runs over 50 ns.

Longer PEG-DME chains, CH_3-(O-CH_2-CH_2)$_n$-O-CH_3, $n = 9, 18, 27, 36, 44, 67, 76$, were also used for comparison to the coarse-grained model. These used respectively, 2940 water molecules for $n = 9, 18, 27$; 10000 water molecules for $n = 36, 44$; 13600 water molecules for $n = 67, 76$. For each chain length, two separate simulations with different initial configurations were used to enhance conformational averaging. After equilibration at constant-*NPT*, constant-*NVT* simulations were carried out using production runs of 30 ns with the final 25 ns used for analysis.

2.2 Coarse-grained simulations

2.2.1 Multiple chains in solution and iterative Boltzmann inversions calculations

GROMACS 4.0.7 was used for the simulation of all coarse-grained systems in this work. Simulations employed numerical potentials for all inter-and intramolecular interactions. Temperature was kept constant at 298 K using a Nosé-Hoover thermostat with a relaxation time of 0.2 ps. Equations of motion were integrated applying the leap-frog algorithm with a time step of 10 fs. A potential cutoff of 16.0 Å was used for nonbonded interactions. Nonbonded potentials for EO-EO sites and for EO-W sites were designed to go smoothly to zero at the cutoff. The nonbonding pair list was updated every 5 time steps with a list cutoff radius of 16.0 Å. Since the van der Waals and electrostatic interactions are incorporated into an effective pairwise potential energy, no electrostatics were present for CG simulations.

The CSJ water ("W" site) developed by Chiu et al.[29] was chosen for CG simulations in this study, after testing a number of different coarse-grained water potentials (see section 2.3 for a description of our choice of water potentials). The repeat unit -CH_2-O-CH_2- (or -CH_2-O-CH_3) (figure 1) was grouped into one coarse-grained site, an "EO" site, to preserve structural symmetry with a coarse-graining level compatible to the CSJ water model. As reported from previous works[23,24,26] this mapping scheme yielded good results for both structural and dynamic properties of PEG in aqueous solution. The CG system used in the iterative Boltzmann inversion process was chosen to mimic the atomistic reference, using 16 chains of PEG10 (10 EO sites per chain) in a box of 38.9 Å/side and 400 water beads (equivalent to 1600 water molecules). Simulations were run under constant-*NVT* conditions for at least 10 ns for each IBI iteration. Further "pressure correction" simulations were carried out under constant-*NpT* conditions as described in the results section.

2.2.2 Single chain in solution

A fully extended PEG-DME chain with a chain length of n = 9 to 200 was first equilibrated using a stochastic dynamics simulation to encourage the chain to adopt a random coil arrangement. For systems of n = 9 to 76, the number of water beads and the box size correspond to those used for the atomistic simulations of section 2.1 (note that one CG water bead is equivalent to 4 atomistic water molecules). For systems of n = 90 to 158, the chain was placed into a box of dimension 125.4 Å/side and solvated by 16400 water beads. The system of n = 200 consists of 27880 water bead in a box of 155.0 Å/side. Two simulations with different initial configurations were performed for each molecular size to enhance sampling. CG simulations were performed under the *NVT* ensemble with 100 ns equilibration and a further 400 ns for data analysis.

2.2.3 Concentration dependence of the radius of gyration for PEG77

CG simulations of PEG-DME at three different concentrations were established by placing 8, 40 and 72 chains of PEG77 into cubic boxes of 20000 water beads of sides 134.3, 136.8 and 139.2 Å respectively, leading to the polymer concentration of 18.6, 88.0 and 150.4 mg cm^{-3}, respectively. Simulations were

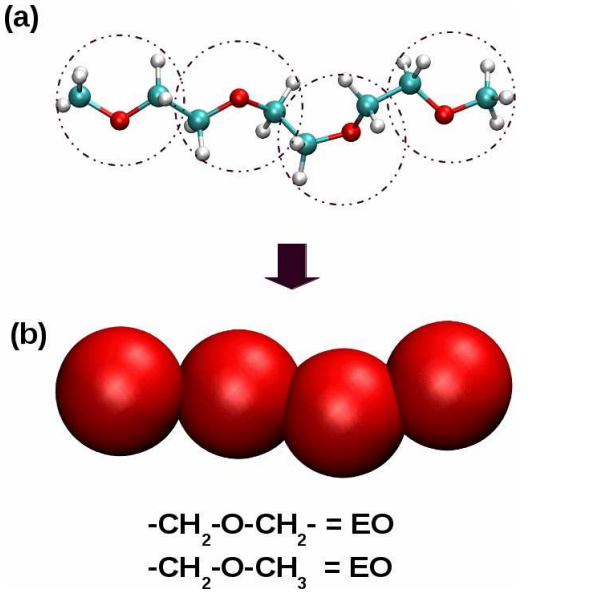

Fig. 1 Atomistic (a) and coarse grained (b) representations of a PEG-DME chain. Each -CH_2-O-CH_2- (or -CH_2-O-CH_3) repeat unit is mapped into one coarse-grained EO site.

conducted under the *NVT* ensemble with a 200 ns equilibration period and a further 500 ns production run.

2.2.4 PEG at a water-air interface

A rectangular box with *x* and *y* dimension of 91 A and *z* dimension of 270 A was first filled with 5000 water beads. The system was subjected to a short *NVT* simulation to allow equilibrated water/vapour interfaces to form (*z* is the axis perpendicular to the surface plane). Ten surface concentrations in polymer were then established by placing one to fourteen chains of PEG77 into the previously equilibrated water slab. The number of PEG77 molecules and the equivalent surface concentration for each system are given in table 1. Note that for the system containing more than ten PEG77 chains, the number of water beads was increased from 5000 to 9000 to provide a water slab thick enough to accommodate all polymer chains. Since there are two interfaces in the simulation box (due to periodic boundaries), PEG chains were placed into the box at positions close to only one side of the water slab to encourage all chains to diffuse to the same surface when they reach equilibrium. This enabled convenient comparisons of results between simulated systems. Once the water/air interface was set up, each system was then subjected to another equilibration run to make sure that it had reached an equilibrium state (i.e. all PEG chains in the system had diffused to the interface and the density distribution of polymer normal to the water surface remained steady). Then, an additional 500 ns was carried out for data analysis. All calculations were performed in the constant-*NVT* ensemble at 298 K.

Table 1 Number of PEG77 molecules and the equivalent surface concentration, Γ_S, for the ten CG simulations at a water-air interface.

PEG77 molecules	* Γ_S / mg m^{-2}
1	0.07
3	0.20
5	0.34
8	0.54
9	0.61
10	0.68
11	0.75
12	0.82
13	0.88
14	0.95

*It is important to note that the surface concentration is calculated on the assumption that all polymer stays at the interface. Experimental reports use the same assumption. This is not strictly true for simulation or experiment for concentrations higher than a saturated monolayer.

2.3 Testing of water potentials

To simulate a PEG model at a water/air interface, we required a suitable CG solvent model capable of representing water in two environments: the bulk and surface. Initially, we tested a series of recently proposed coarse-grained water potentials to see if they could meet this requirement. Calculations were run for bulk water and for a slab of water with an initial vacuum interface, employing 10000 particles and a Langevin thermostat with a friction coefficient of 5 ps^{-1}.

The numerical potentials by Wang et al.[41] (WJK) and Lyubartsev et al.[42] (LMCL) both use a single spherical site to represent one water molecule (1:1 mapping). These work well in terms of reproducing water structure (e.g. the radial distribution function (RDF)) and some thermodynamic properties of water. Unfortunately, our tests showed that neither potential was able to represent liquid/vapour equilibrium. Both were unable to maintain two separate phases at room temperature with a sharp interface (see supplementary material). The WJK and LMCL potentials were originally obtained from fitting to atomistic RDFs. In an attempt to improve the potentials, we refitted them using a long range attractive tail, following the iterative Boltzmann inversion methodology of Wang et al. [41]. This procedure allowed us to obtain a potential that increased the surface tension of liquid water and supported liquid/vapour coexistance by extending the weakly attractive tail to 14 Å. However, the unrealistic width of the interface produced for

this extended potential (several nanometers), made us conclude that it was not feasible to use a water potential based on 1:1 mapping and RDF fitting for the current study.

The next set of water models we studied were all analytical potentials of the Mie/Lennard-Jones (LJ),

$$U = A/r^n - B/r^m, \quad (1)$$

or Morse,

$$U = \varepsilon \left[\exp\left(\alpha\,(1 - r/R_0) - 2\exp\left(\frac{1}{2}\alpha\,(1 - r/R_0) \right) \right) \right] \quad (2)$$

forms: the LJ 6:4 SSRBK model developed by the Klein group[27,43], the LJ 12:6 MARTINI water by Marrink and coworkers[16,44] and the CSJ water by Chiu et al.[29]. These models (see supplementary material) all use one pairwise interaction site to represent a group of three[43] or four[29,44] water molecules. This type of model is designed for simulations of systems involving a large number of solvent molecules, as the high degree of coarse-graining provides a significant speed-up in simulations compared to that provided by the WJK/LMCL approach. These coarser-grained models are usually developed using thermodynamic properties of water (for example, the experimental density, the water-vapour surface tension and the heat of vaporization) as targets.

We performed tests of each CG water to examine their liquid-vapour interfacial behaviour. All three models succeeded in maintaining very resonable liquid-vapour density profiles, compared to atomistic simulations of TIP4P-Ew water (see supplementary material). However, MARTINI water was found to have a low surface tension compared to experiment, partly because the attractive well is both deep and short range (this can also lead to aggregation or freezing at an interface).The CSJ and SSRBK potentials are both softer than the MARTINI model (see supplementary material). Not only does this discourage freezing, it also means a larger integration time step can be employed (e.g. 40 fs for CSJ). The CSJ and SSRBK water models both have calculated surface tensions of 71 mN/m at 298 K[29], in good agreement with the experimental value of 73 mN/m. However, the heat of vaporization is better reproduced by CSJ water. (The SSRBK model considerably underestimates the experimental value[29]). We found that this was also reflected in a rather high vapour pressure in simulations of the SSRBK model at room temperature. Moreover, the CSJ model works with a shorter potential cutoff (cuttoff 16 Å) and a higher degree of mapping (4:1), and thus, promotes faster calculation than the SSRBK model (cutoff 18.8 Å,mapping 3:1). Based on the results discussed here, the CSJ potential proved the best choice for futher polymer/water simulations.

We note in passing that a number of coarse-grained models have recently been developed for water, which introduce orientational polarizability[45–47]. These models explicitly treat the electrostatic interactions between clusters of water molecules by including a dipole (arising from 2 or 3 charge sites on one CG bead). While, these models have the disadvantage of adding computational expense through the introduction of long range interactions, it will be interested to see if they are able to provide improved CG models for polymer in aqueous solution in future studies, in comparison to the work presented here.

3 Results and Discussion

3.1 Derivation of coarse-grained potentials for PEG in water

The coarse-grained PEG chain used (figure 1) was modelled via four types of interactions: nonbonded, bond stretching, bond bending and dihedral. Nonbonded interactions were applied for CG beads separated by more than two bonds. Dihedral terms are often not required in coarse-grained models. However, the use of explicit dihedral potentials here, arises from the suggestion in previous work[23,24] that these terms would need to be included in the potential set for PEG chains in order to reproduce *gauche*-like conformations observed in atomistic simulations. The bonded potentials were derived on the basis of matching the distribution functions to those of the atomistic reference. Interactions between EO sites were derived from the radial distribution function (RDF) between the centre of mass of the C-O-C units from atomistic simulation using the iterative Boltzmann inversion technique. Since each W site in the CSJ model represents four water molecules, comparison between CG and atomistic RDFs cannot be made for EO-W interactions, because the EO-water atomistic RDF cannot be represented within the 4:1 CG mapping. To this end, we chose to match the number integral of the RDF between CG and atomistic models in order to keep approximately the same amount of water in the hydration shell of the polymer units. This is a similar approach to that applied in the coarse-graining of a phospholipid bilayer model by Shelley et al.[43]. A set of CG potentials was derived by successively adjusting the different potential contributions in the order of their relative strengths: $U_{\text{stretch}} \rightarrow U_{\text{bend}} \rightarrow U_{\text{nonbonded}} \rightarrow U_{\text{dihedral}}$. This is an efficient way of obtaining CG potentials with the IBI technique, since "harder potentials" are matched first and it has already been shown from previous work that the intramolecular degree of freedoms can be treated almost independently from intermolecular ones[20,23].

Figure 2 shows an excellent match of the bond-, angle- and dihedral angle distributions. All fits required only a few steps of iteration to converge from initial guesses based on Boltzmann- inverted potentials of the target bond, angle and dihedral distributions.

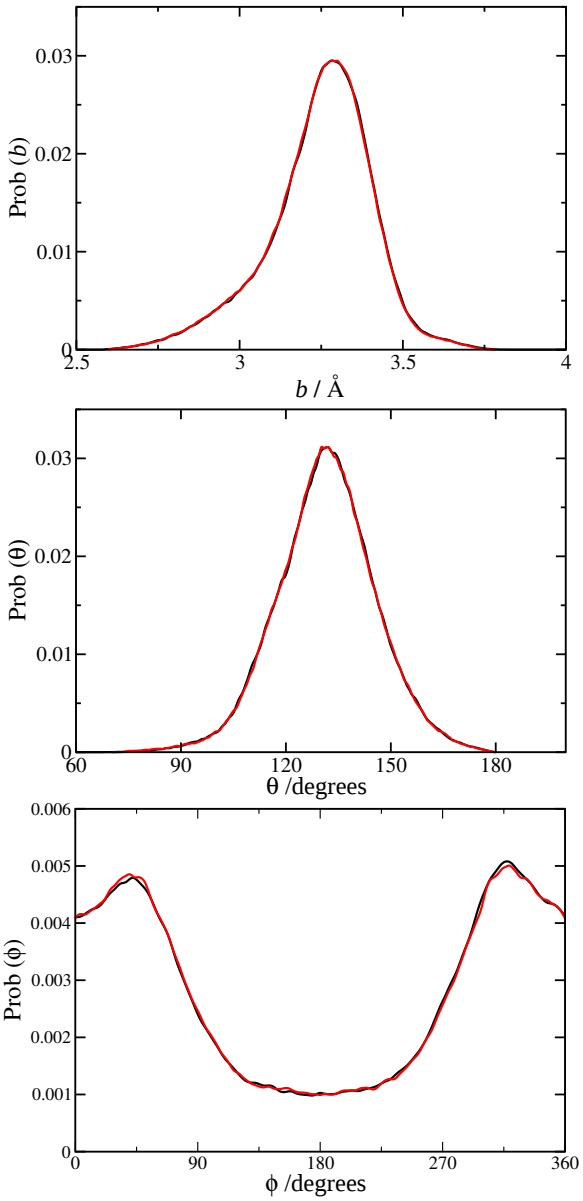

Fig. 2 Probability distributions of bond lengths (top), bond angles (middle), and dihedral angles (bottom) of PEG10 from atomistic simulation (black) and coarse-grained simulation at the final Boltzmann iteration step (red).

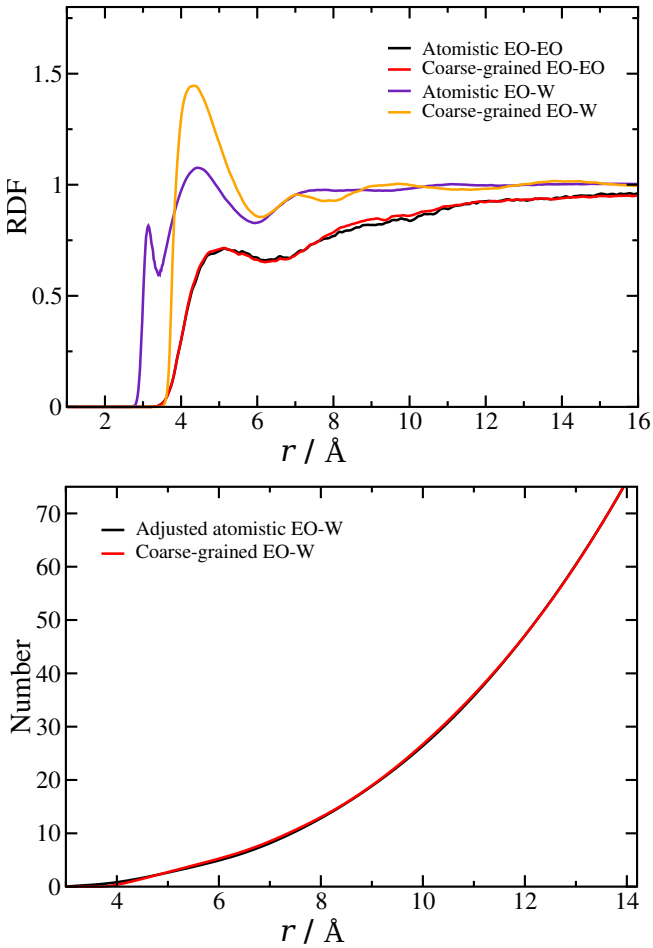

Fig. 3 Top: radial distribution functions for the EO-EO sites, atomistic (black) and CG (red) and the EO-W sites, atomistic (violet) and CG (orange). Bottom: number integrals of RDF_{EO-W}, atomistic (black) and coarse-grained (red). The adjusted atomistic integral is one-fourth of the atomistic integral since each W site represents four water molecules.

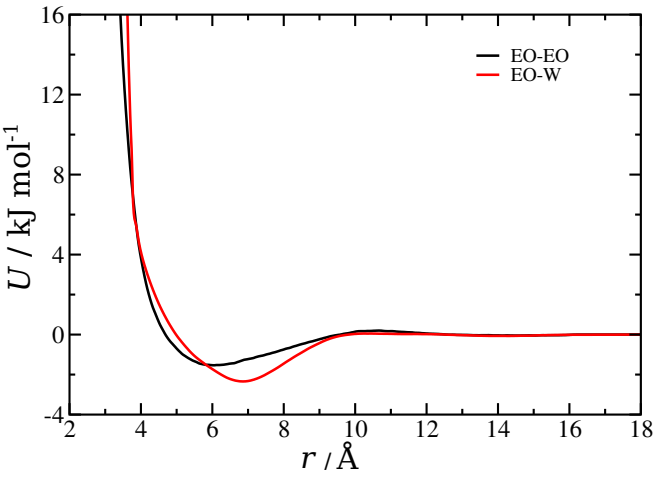

Fig. 4 Nonbonded potentials between EO-EO sites (black) and EO-W sites (red) obtained from the final Boltzmann iteration with pressure correction.

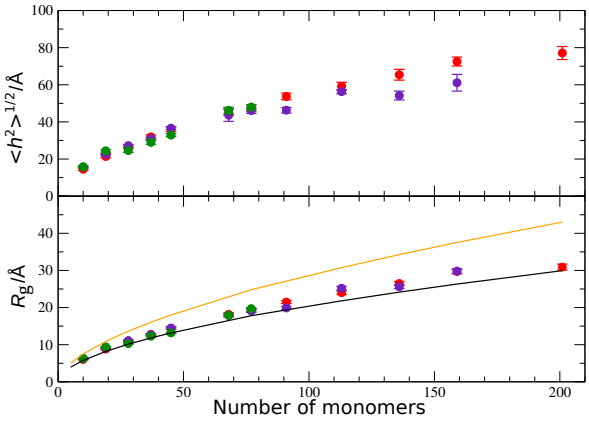

Fig. 5 Molecular weight dependence of chain dimension for PEG in aqueous solution. (Top) mean-squared end-to-end distance $<h^2>^{1/2}$ from coarse-grained simulations (red), atomistic simulations (green), and the coarse-grained MARTINI model, taken from Lee et al.[24] (violet). (Bottom) Radius of gyration R_g from coarse-grained simulations (red), atomistic simulations (green), and the coarse-grained MARTINI model, taken from Lee et al.[24](violet). The green and orange lines in the plot are calculated by extrapolation of experimental data by Kawaguchi et al.[48] and Devanand and Selser [49].

For the nonbonded interactions, it was not feasible to perfectly match both the $RDF_{EO\text{-}EO}$ and the number integral of the $RDF_{EO\text{-}W}$ to their targets at the same time. This is because the two nonbonded potentials can have an effect on the structure of each other. For example, changing the EO-W potential was found to lead to dramatic changes in the $RDF_{EO\text{-}EO}$. However, overall good fits were obtained by allowing $RDF_{EO\text{-}EO}$ to deviate very slightly from the target in order to maintain a good fit for both $RDF_{EO\text{-}EO}$ and the number integral of the $RDF_{EO\text{-}W}$. Figure 3 compares the atomistic and the final coarse-grained RDFs for the EO-EO and EO-W sites. For the $RDF_{EO\text{-}EO}$, the match is excellent with only a very minor discrepancy at a distance around 8 to 10 Å.

It is important to note that $RDF_{EO\text{-}W}$ does not (by design) pick up the fine detail in the atomistic RDF for EO-Oxygen(H_2O) because of the 4:1 mapping of water sites. Subtle changes in the first peak of the atomistic reference EO-Oxygen RDF, can, in principle, indicate changes in hydrogen bonding between water molecules and EO sites. We therefore expect such effects to be lost at this level of coarse-graining. The number integral for EO-W pairs in the atomistic and CG simulation are also plotted in figure 3. The match of the number integral is excellent for the whole range of the distance observed. This assures that we have obtained approximately the same level of hydration of the EO site in the CG and atomistic simulation, which is essential for the model we use.

The structural optimisation discussed above was run at constant volume and without long-range correction for the nonbonded interactions. This causes a large deviation between the pressure of the CG simulation ($p \approx$ 850 bar) and the underlying atomistic system ($p \approx$ -180 bar). We therefore carried out pressure correction for the CG system by introducing an attractive linear tail function to the previous optimized nonbonded potentials[20]. The correction to the potential, $\Delta U(r) = A_0\left(1 - \frac{r}{r_{\text{cutoff}}}\right)$, fulfills the following essential conditions: $\Delta U(r=0) = A_0$ and $\Delta U(r_{\text{cutoff}}) = 0$. The corrected potentials are then taken as an initial guess for a re-optimisation of the potentials against the structure using the IBI method. After that, the pressure is re-evaluated and the procedure continued until convergence has occurred. By this correction the CG pressure was successfully reduced to approximately -170 bar. The nonbonded potentials obtained from the final correction are shown in figure 4. The coarse-grained EO-EO potential shows three characteristic features, including a first minimum around 6 Å, a small repulsive midrange region and a very weakly attractive tail. For the EO-W potential, the first minimum appears at quite a large distance (7 Å). This can be attributed to the large size of the W particle (in this case, representing four water molecules), preventing its centre coming as close to the polymer units as a single water molecule could. The potential well for this interaction is, however, relatively deep, leading to strong solvation of water beads around the polymer unit.

3.2 Molecular weight dependence of chain dimension

The dependence of chain dimension, in terms of radius of gyration R_g and end-to-end distances $<h^2>^{1/2}$ are plotted in fig-

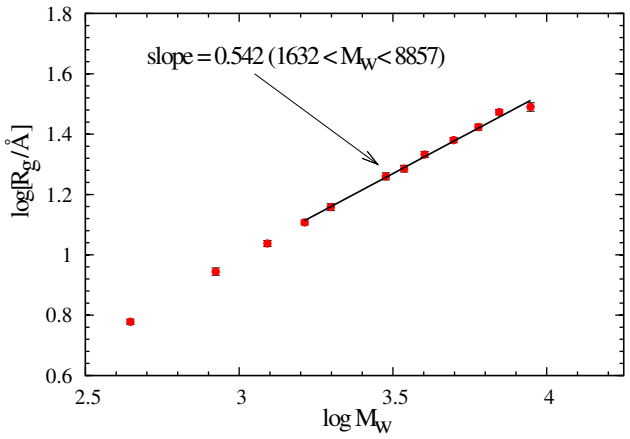

Fig. 6 log R_g versus log M_W from simulations of a single PEG-DME chain in aqueous solution with $1632 < M_W < 8857$.

ure 5 (a) and (b), in terms of number of monomers. Results from atomistic simulations and from the MARTINI model[24] are also included for comparison. The overall R_g and $<h^2>^{1/2}$ are in good agreement with atomistic calculations and the MARTINI model except for $M_W > 3438$ (> 77 monomers) where our model yields slightly larger end-to-end distances than the MARTINI model. The calculated R_g for PEG77 is 19.3 ± 0.4 Å, in excellent agreement with the value of 19.1 ± 0.7 Å from the CG MARTINI model and the value of 19.7 Å from neutron scattering measurements of poly(ethylene glycol) (PEG) of equivalent molecular weight at low concentration[50].

A least squares fit from the plot of log R_g against log M_W in 6 gives a power law relation of $R_g = 0.235 M_W^{0.542}$ for $1632 < M_W < 8857$. This result is in good agreement with a relation of $R_g = 0.202 M_W^{0.550}$ from light scattering measurement by Kawaguchi et al.[48], but shows lesser expansion of the chain compared to light scattering result by Devanand and Selser ($R_g = 0.215 M_W^{0.583 \pm 0.031}$)[49], also shown in figure 5. The scaling law reported by Devanand and Selser was fitted for high M_W (10^5 to10^6), while the M_W-dependence of R_g by Kawaguchi et al. was determined from low to high M_W (10^2 to 10^7). The M_W used in our simulations is in the range studied by the latter, thus, it is reasonable that our results compare more favourably with the Kawaguchi et al. data. For comparison, the coarse-grained PEG model by Fisher et al.[23] yield the relation $R_g = 0.326 M_W^{0.537}$ from simulations of $4407 < M_W < 66082$, the MARTINI model gives $\nu = 0.57 \pm 0.02$ from a fit for $1630 < M_W < 6998$.

3.3 Concentration Dependence of Radius of Gyration

Decreases in R_g with increasing polymer concentration have been reported by small angle neutron scattering (SANS) measurements[50,51]. SANS measurements on PEG77 revealed a sharp decrease in the apparent R_g from 19.7 Å at 30 mg cm^{-3} to 8.0 Å at 160 mg cm^{-3}[50]. Changes in the three-dimensional structure[51] and repulsive intermolecular interactions (excluded volume effects) at high concentration are possible explanations for this. However, there is no evidence of a reduction of R_g at higher concentration as studied by the recent atomistic and the CG simulations[23,24]. Figure 7 plots the average R_g as a function of simulation time for PEG77 at three concentrations. From figure 7, there is no significant difference in the time taken for the chains to equilibrate. For all systems, R_g reached equilibrium values very quickly, within 10 ns. $\langle R_g \rangle$ for concentrations of 18.6, 88.0 and 150.4 mg cm^{-3} are 19.4 ± 0.2, 19.2 ± 0.1 and 19.1 ± 0.2 Å, respectively. Thus, in our model up to the concentrations studied, R_g appears not to be dependent on polymer concentration. It remains unclear whether there is a disagreement with results obtained from SANS and simulation studies. As noted by Lee et al.[24], apparent decreases of R_g at high concentration might arise from interchain scattering. The supporting reason for this is that SANS spectra are expected to be sensitive to an isolated coil, which should provide reliable value of R_g in very dilute solutions[52]. At higher concentrations the polymer coils begin to entangle and the identities of the individual polymer coils may be lost[53]. The apparent R_g values obtained at high concentrations are typically to be replaced by static correlation lengths[51].

It is important to note that a number of additional factors may influence experimental PEG/water systems. For example, it is known that PEG chains bind efficiently to alkali metal ions, which are present in trace quantities even in distilled water, and are usually not completely removed from PEG reagents. Moreover, most commercially available PEGs have some degree of polydispersity. The influence of both these factors are not yet known but would be interesting to model.

3.4 PEG77 at a Water-Air Interfaces

3.4.1 General Observations

Although PEG/PEO is water soluble, (due to its lower surface energy compared to that of pure water) it has also been shown to form stable spread films at the water-air interface under certain circumstances[54–56]. The -CH_2-O-CH_2- component is sufficiently hydrophobic to escape from the water subphase and to form an adsorbed layer at a surface. This structure is energetically preferable and this disturbs the hydrogen bonded network of water at the surface and as a result, the surface tension of the system drops in the presence of this surfactant[56–59]. It has also been suggested from experiment that at higher surface concentrations polymer segments extend into the water subphase as loops and tails. This extension increases as sur-

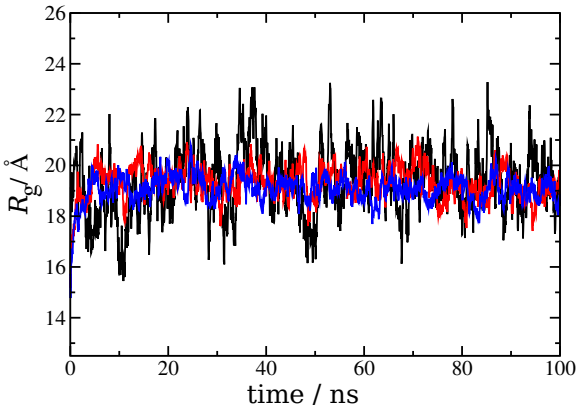

Fig. 7 Time series of the radius of gyration R_g for PEG77 at concentration of 18.6 mg cm^{-3} (black), 88.0 mg cm^{-3} (red) and 150.4 mg cm^{-3} (blue).

face concentration increases[55]. From the simulation point of view, it is worth examining the transferability of our coarse-grained model in terms of capturing adsorption, as discussed above.

Figure 8 shows the final configuration from the simulation of 10 chains of PEG77 ($\Gamma_S = 0.68$ mg m^{-2}) at the water-air interface. It is clearly shown that PEG-DME chains form a layer at the water surface, in accordance with the interpretation of experimental observations. Observing trajectory movies through the course of the simulation, shows that PEG chains diffuse quickly from the bulk water phase to the interface region. After reaching the water surface, chains align themselves along the surface plane, and a polymer layer is formed that persists until the end of the simulation.

3.4.2 Density Profiles

Mass density profiles of EO normal to the surface for ten surface concentrations are plotted in figure 9. At low polymer concentrations (0.07-0.34 mg m^{-2}), almost all the polymer segments locate at or just beneath the liquid surface. However, there is shown to be a small fraction of the polymer penetrating into the vapour phase, as shown in figure 10 (a). This behaviour has also been reported by recent atomistic simulation of PEG50 at a free water surface ($\Gamma_S \approx 0.4$ mg m^{-2})[60], suggesting that about 1% of the monomer units penetrate into the vapour phase.

The surface region gets more occupied by EO segments as the concentration of polymer is increased. Formation of a EO layer at the interface is energetically favourable, resulting in water being excluded from the interface and pushed down into the subphase region. Figure 10 (b) shows the final structure obtained from simulation of the system of 10 PEG77 molecules (Γ_S = 0.68 mg m^{-2}). Here, a smaller amount of water penetrates into the polymer layer compared to the lower

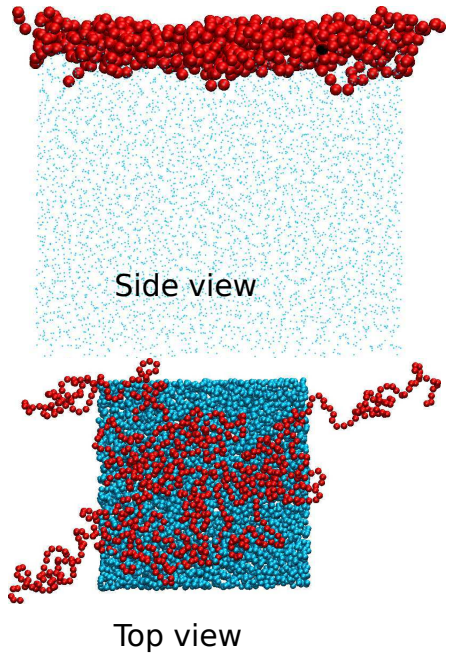

Fig. 8 Side view and top view of the final structure obtained from the simulation of 10 coarse-grained molecules of PEG77 (0.68 mg m^{-2}) at a water-air interface. Red spheres represent EO groups, water molecules are shown in blue as dots (in the side view) or spheres (in the top view).

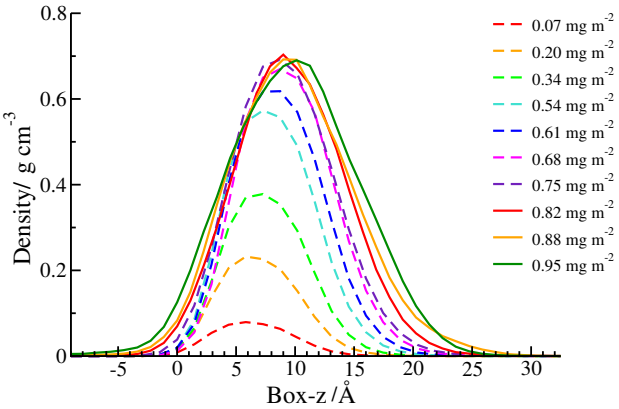

Fig. 9 Density profiles of PEG-DME from the simulations of ten systems with the surface concentration ranging from 0.07 to 1.09 mg m^{-2}. A polymer layer is formed at the interface region and the left-hand side (-z) and right-hand side (+z) approximately represent air- and bulk water phase, respectively.

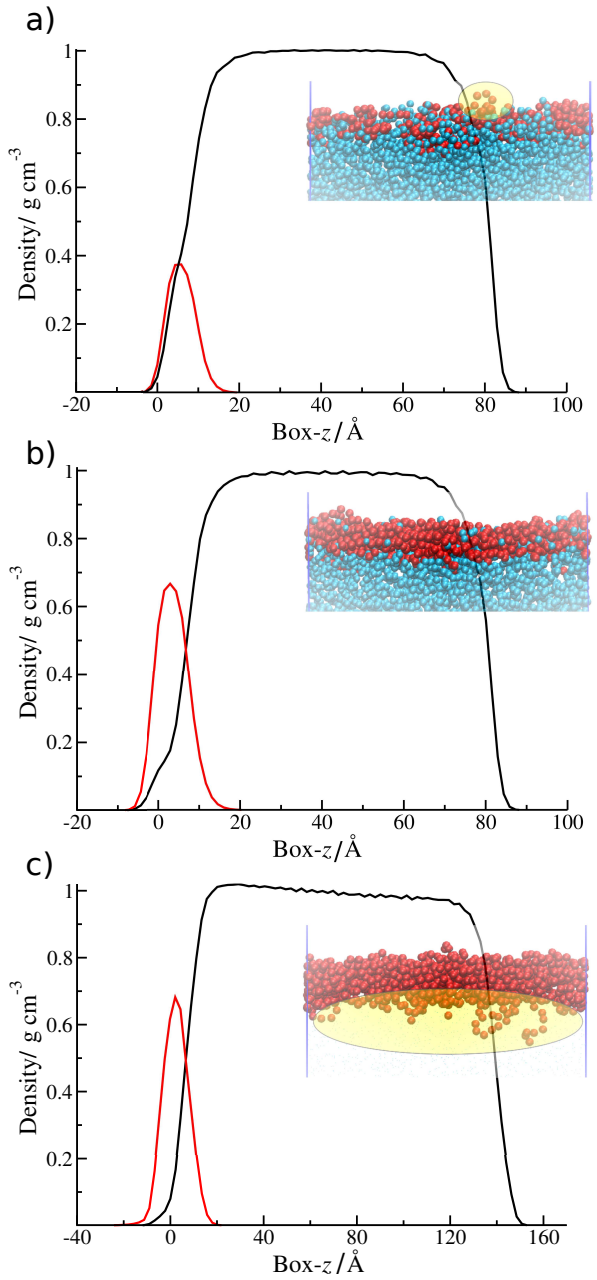

Fig. 10 Density profiles and typical snapshot pictures obtained from simulations of (a) 5 chains (0.34 mg m^{-2}), (b) 10 chains (0.68 mg m^{-2}) and (c) 14 chains (0.95 mg m^{-2}) at a water-air interface. The red line shows the density of EO groups and the black line shows the density of water molecules. In the snapshots, red spheres represent EO groups and water molecules are shown (in (a) and (b) only) in blue. The highlight in (a) shows EO segments penetrating into the vapour phase and in (c) shows extension of EO segments into the water subphase as loop and tail conformations.

concentration system in figure 10 (a). Correspondingly, the water density profile in figure 10 (b) shows depletion in the interface region.

Adsorption of PEG-DME at the surface continues to increase with increasing polymer concentration until a surface concentrations of 0.68 mg m^{-2} above which the amplitudes of the density profiles at the surface are essentially unchanged; but do show an extension of PEG segments into the subphase. This indicates that there is no more space for more EO segments to pack at the surface. Based on the calculated density profiles, the monolayer is thus suggested to be completed at a concentration around 0.68 mg m^{-2}. This surface coverage agrees almost exactly with the value of 0.7 mg m^{-2} obtained from neutron reflection measurement by Rennei et al.[54], and agrees also with results from surface pressure isotherm measurements at ambient temperature[61–63]. However, we note that slightly lower values, with a monolayer completed between 0.5 and 0.6 mg m^{-2} were obtained from neutron reflectometry measurements by Henderson et al.[55] and Lu et al.[56]. This difference of surface excess from experiments is outside the experimental error and has been noted to be due to the properties of PEG films that are sensitive to the molecular weight used in each study[56,63,64]. We note that the molecular weight of chains used in our simulation study is lower than used in experiments, and so we expect a slightly larger surface concentration to be possible in the simulations.

For surface concentrations above 0.68 mg m^{-2}, the aqueous subphase can no longer accommodate more EO segments at the surface. As a result, the excess polymer, above the amount required to form a monolayer, extends into the aqueous subphase, as shown in the density profiles (figure 9). "Extension" or "collapse" of PEG/PEO monolayers has previously been proposed in experiments[55,61,62,65,66]. From neutron reflectometry of high molecular weight PEO by Henderson et al.[55], the saturation of the monolayer was attained at surface concentrations of approximately 0.5 mg m^{-2}. Increasing surface concentration above 0.5 mg m^{-2} did not change the number density of EO segments in the topmost layer, but resulted in increasing extension of the lower polymer layer into the liquid subphase, probably as loop and tail conformations. Kuzmenka and Granick[61,62,66] noted that at low surface concentration there was a loss of entropy due to confinement of the molecules to two dimensions along the interface. At higher surface coverages there was a gain in entropy as the monolayer collapsed to a three-dimensional structure (buckling and looping into the water subphase). Kawaguchig et al.[67] and Rennie et al.[54] have also mentioned loop and tail conformations for a high surface concentration regime. Unfortunately, there are no direct experimental methods to demonstrate the occurrence of these conformational features. However, a snapshot from the final configuration of the system with 14 polymer chains (Γ_S = 0.95 mg m^{-2}), in which the density profile has already shown

to be collapsed from the saturation point (figure 10) shows the presence of both loop and tail conformations of the polymers very clearly.

The layer thickness of the PEG-DME monolayer is also interesting to consider as this reflects the organization of polymers at the water-air interface. The polymer layer is known to be rather flat and can be classified as a pancake organization rather than a brush-like layer[55,56,68]. By analyzing neutron reflectivity data, Henderson et al.[55] reported the layer thickness of 16 ± 2 Å, 19 ± 2 Å and 22 ± 2 Å for the surface concentration of 0.5 mg m^{-2}, 0.6 mg m^{-2} and 0.8 mg m^{-2}, respectively. The thickness of 23 ± 2 Å for the concentration of 0.6 ± 0.1 mg m^{-2} was reported by Lu et al.[56] As approximated from the density profiles in figure 9, the layer thickness of the PEG layer is found to be around 18 Å , 19 Å and 24 Å respectively for the concentration of 0.54 mg m^{-2}, 0.61 mg m^{-2} and 0.82 mg m^{-2}. The PEG layer thicknesses from our simulations are therefore in good agreement with results from neutron reflectometry for the same surface concentration range.

3.5 Speed-up of the Coarse-Grained Model

In coarse-grained models, removing degrees of freedom will also remove their friction contribution, and thus, speed up the dynamics. In PEG/water, this includes the loss of specific strong site-site interactions, such as the hydrogen bonding interaction between the ether oxygens in PEG and water molecules. This reduction in friction turns out to be extremely useful for studying polymer self-assembly at a water surface since fast diffusion and relaxation of chains are required for fast equilibration. In this study the speed-up of the CG model was tested by measuring the time required by the system to equilibrate a polymer layer at a water/air surface. (We note in passing that there is absolutely no guarantee that different dynamical processes are speeded up by the same amount in the process of coarse-graining. So some degree of caution must be exercised in using coarse-graining to "observe" dynamical processes that can not be seen in atomistic simulations.)

To compare equilibration times, we used an atomistic model of 10 randomly placed relaxed PEG77 chains in a slab of 20000 water molecules with box dimensions $x = y = 86.5$ Å and $z = 286.5$ Å (z is the axis perpendicular to the surface plane); and extracted the CG starting structure directly from the starting atomistic coordinates. Simulations were performed on the same processors, i.e. a parallel molecular dynamics on 32 compute nodes.

In this study it took more than 50 ns for all atomistic PEG chains to move slowly from the bulk liquid phase to the interface regions and form a stable layer there. This phenomena happened very quickly for the CG system, where all the chains reach the surface within 5 ns. Figure 11 compares the variation in z-component of the radius of gyrations ($R_{g,z}$) for atomistic and CG systems. At the start of the simulation, polymer chains in the liquid phase can freely move along the z-dimension toward the interfaces, resulting in a large fluctuation of $R_{g,z}$ at this point. After the system has reached equilibrium, the $R_{g,z}$ value should remain steady since molecules are confined in a two dimensional (x-y) layer at the interface. Thus, following the variation in $R_{g,z}$ with time seems to be a suitable choice to detect the true equilibration time taken by both systems. As shown in figure 11 the mean $R_{g,z}$ has reached equilibrium at simulation times of ≈ 55 ns and ≈ 4 ns for atomistic and CG chains, respectively. Thus, the CG model can relax approximately 14 times faster than the atomistic model in terms of raw time. However, the reduction in sites within the CG model, together with a 5-fold increase in time step, means that the total speed up for equilibration is by a factor of 1,042$\times$ in terms of real computer time. Although, we were unable to equilibrate longer atomistic model chains to check, we would expect an even greater speed-up to be achieved with our coarse-grained model for equilibration of long chains.

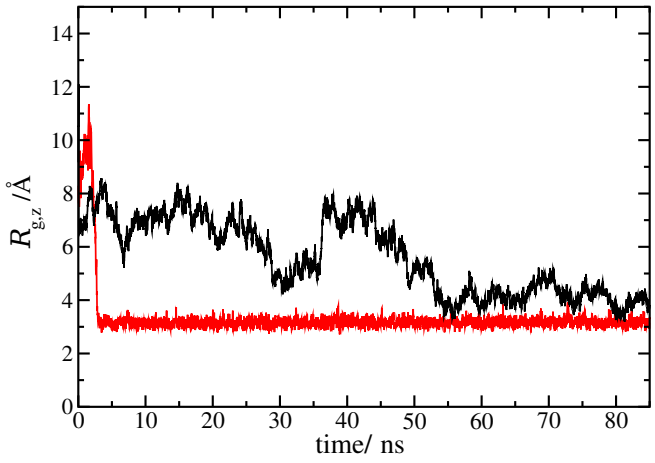

Fig. 11 Time evolution of the radius of gyration along the z-direction ($R_{g,z}$) for PEG-DME chains in atomistic (black) and CG (red) simulations at a water-air interface.

4 Conclusions

A coarse-grained model for poly(ethylene glycol)dimethylether (PEG-DME), CH_3-[O-CH_2-CH_2]$_n$-O-CH_3, has been presented, using coarse-grained potentials derived using the iterative Boltzmann inversion technique. The model provides an excellent match between radial distribution functions (and distributions of bonds, angles and dihedrals) of coarse-grained and atomistic reference simulations.

Simulations of a single chain in aqueous solution with PEG, molecular weights from 442 to 8857, showed successful reproduction of the experimental scaling laws for the radius

of gyration R_g. The simulated R_g for PEG77 ($M_W \approx 3400$) is in excellent agreement both with the CG MARTINI model and neutron scattering result for an equal sized poly(ethylene glycol) chain. The concentration dependence of the radius of gyration has also been investigated using PEG77. Our simulations showed no reduction of R_g with increases in polymer concentrations, in agreement with results from previous atomistic and coarse-grained simulations, but in contradiction to reported experimental observations where the apparent R_g is shown to decrease drastically as concentration changed from low to high.

Without any modification, the CG model derived from aqueous solution conditions was used in water/air interface simulations to test its transferability. A series of simulations with surface concentration ranging from the low to high, using a PEG chain of 77 monomers were performed. At the simulated temperature of 298 K, polymer chains are shown to diffuse from the water subphase to form a monolayer at the water-air interface, and the surface excess was found to increase with increasing polymer concentration. Results for the saturation adsorption, and the thickness of polymer layers obtained from CG simulations, are in good agreement with experimental findings. As polymer concentration increases above the saturation adsorption, the monolayer is shown to collapse to a three-dimensional structure by tailing and looping into the water subphase. This extension of polymer segments increases as the polymer concentration increases.

The present model is also shown to provide very fast diffusion and relaxation of polymers in the adsorption process. Comparing to a similar sized atomistic system, the coarse-grained model provided a 1,042x speed-up in the equilibration process.

We conclude that, for PEG chains in water, the IBI technique combined with the CSJ water potential provides a very promising model to study adsorption behaviour of long PEG chains, and can be used in bulk solution and at a water/air interface. We also suggest that the approach used here could easily be extended to study amphiphilic PEG chains tethered at a water surface. Such systems have been difficult to simulate previously with atomistic models[68,69], since they cannot relax highly crowded configurations within accessible simulation times but may now be studied using the coarse-grained approach described here.

References

1 G. N. Malcolm and J. S. Rowlinson, *Trans. Faraday Soc.*, 1957, **53**, 921–931.
2 G. N. I. Clark, A. Galindo, G. Jackson, S. Rogers and A. N. Burgess, *Macromolecules*, 2008, **41**, 6582–6595.
3 S. Y. Oh, H. E. Yang and Y. C. Bae, *Macromolecular Research*, 2013, **21**, 921–930.
4 H. J. M., *Poly(Ethylene Glycol) Chemistry: Biotechnical and Biomedical Applications*, Springer, 1992.
5 P. Alexandridis and T. A. Hatton, *Colloids and Surfaces A: Physicochemical and Engineering Aspects*, 1995, **96**, 1 – 46.
6 F. M. Veronese and G. Pasut, *Drug Discovery Today*, 2005, **10**, 1451 – 1458.
7 F. Chami, M. R. Wilson and V. S. Oganesyan, *Soft Matter*, 2012, **8**, 6823–6833.
8 F. Chami and M. R. Wilson, *J. Am. Chem. Soc.*, 2010, **132**, 7794–7802.
9 A. Lukyanov, A. Malafeev, V. Ivanov, H.-L. Chen, K. Kremer and D. Andrienko, *J. Mater. Chem.*, 2010, **20**, 10475–10485.
10 J. Pelaez and M. Wilson, *Phys. Chem. Chem. Phys.*, 2007, **9**, 2968–2975.
11 C. Peter and K. Kremer, *Soft Matter*, 2009, **5**, 4357–4366.
12 C. Peter and K. Kremer, *Faraday Discuss.*, 2010, **144**, 9–24.
13 P. Carbone, H. A. K. Varzaneh, X. Y. Chen and F. Muller-Plathe, *J. Chem. Phys.*, 2008, **128**, 064904.
14 S. Izvekov and G. A. Voth, *J. Chem. Phys.*, 2005, **123**, 134105.
15 W. G. Noid, J. W. Chu, G. S. Ayton and G. A. Voth, *J. Phys. Chem. B*, 2007, **111**, 4116–4127.
16 S. J. Marrink, H. J. Risselada, S. Yefimov, D. P. Tieleman and A. H. de Vries, *J. Phys. Chem. B*, 2007, **111**, 7812–7824.
17 F. Muller-Plathe, *Chemphyschem*, 2002, **3**, 754–769.
18 L. Stimson and M. Wilson, *J. Chem. Phys.*, 2005, **123**, 034908.
19 Q. Wang, D. J. Keffer and D. M. Nicholson, *J. Chem. Phys.*, 2011, **135**, 214903.
20 D. Reith, M. Putz and F. Muller-Plathe, *J. Comput. Chem.*, 2003, **24**, 1624–1636.
21 V. Ruehle, C. Junghans, A. Lukyanov, K. Kremer and D. Andrienko, *J. Chem. Theory Comput.*, 2009, **5**, 3211–3223.
22 C. X. Chen, P. Depa, V. G. Sakai, J. K. Maranas, J. W. Lynn, I. Peral and J. R. D. Copley, *J. Chem. Phys.*, 2006, **124**, 234901.
23 J. Fischer, D. Paschek, A. Geiger and G. Sadowski, *J. Phys. Chem. B*, 2008, **112**, 13561–13571.
24 H. Lee, A. H. de Vries, S. J. Marrink and R. W. Pastor, *J. Phys. Chem. B*, 2009, **113**, 13186–13194.
25 G. Rossi, P. F. J. Fuchs, J. Barnoud and L. Monticelli, *J. Phys. Chem. B*, 2012, **116**, 14353–14362.
26 D. Bedrov, C. Ayyagari and G. D. Smith, *J. Chem. Theory Comput.*, 2006, **2**, 598–606.
27 G. Srinivas, J. C. Shelley, S. O. Nielsen, D. E. Discher and M. L. Klein, *J. Phys. Chem. B*, 2004, **108**, 8153–8160.
28 W. Shinoda, R. DeVane and M. L. Klein, *Soft Matter*, 2008, **4**, 2454–2462.
29 S. W. Chiu, H. L. Scott and E. Jakobsson, *J. Chem. Theory Comput.*, 2010, **6**, 851–863.
30 B. Hess, C. Kutzner, D. van der Spoel and E. Lindahl, *J. Chem. Theory Comput.*, 2008, **4**, 435–447.
31 J. Fischer, D. Paschek, A. Geiger and G. Sadowski, *J. Phys. Chem. B*, 2008, **112**, 2388–2398.
32 H. W. Horn, W. C. Swope, J. W. Pitera, J. D. Madura, T. J. Dick, G. L. Hura and T. Head-Gordon, *J. Chem. Phys.*, 2004, **120**, 9665–9678.
33 J. M. Stubbs, J. J. Potoff and J. I. Siepmann, *J. Phys. Chem. B*, 2004, **108**, 17596–17605.
34 P. M. Anderson and M. R. Wilson, *Mol. Phys.*, 2005, **103**, 89–97.
35 R. W. Hockney, S. P. Goel and J. W. Eastwood, *J. Comput. Phys.*, 1974, **14**, 148–158.
36 S. Nose, *Mol. Phys.*, 1984, **52**, 255–268.
37 W. G. Hoover, *Phys. Rev. A*, 1985, **31**, 1695–1697.
38 M. Parrinello and A. Rahman, *J. Appl. Phys.*, 1981, **52**, 7182–7190.
39 U. Essmann, L. Perera, M. L. Berkowitz, T. Darden, H. Lee and L. G. Pedersen, *J. Chem. Phys.*, 1995, **103**, 8577–8593.
40 B. Hess, H. Bekker, H. J. C. Berendsen and J. G. E. M. Fraaije, *J. Comput.*

Chem., 1997, **18**, 1463–1472.
41 H. Wang, C. Junghans and K. Kremer, *Eur. Phys. J. E*, 2009, **28**, 221–229.
42 A. Lyubartsev, A. Mirzoev, L. Chen and A. Laaksonen, *Faraday Discuss.*, 2010, **114**, 1–14.
43 J. C. Shelley, M. Y. Shelley, R. C. Reeder, S. Bandyopadhyay and M. L. Klein, *J. Phys. Chem. B*, 2001, **105**, 4464–4470.
44 S. J. Marrink, A. H. de Vries and A. E. Mark, *J. Phys. Chem. B*, 2004, **108**, 750–760.
45 Z. Wu, Q. Cui and A. Yethiraj, *J. Phys. Chem. B*, 2010, **114**, 10524–10529.
46 S. O. Yesylevskyy, L. V. Schafer, D. Sengupta and S. J. Marrink, *PLoS Comput. Biol.*, 2010, **6**, e1000810.
47 S. Riniker and W. F. van Gunsteren, *J. Chem. Phys.*, 2011, **134**, 084110.
48 S. Kawaguchi, G. Imai, J. Suzuki, A. Miyahara and T. Kitano, *Polymer*, 1997, **38**, 2885–2891.
49 K. Devanand and J. C. Selser, *Macromolecules*, 1991, **24**, 5943–5947.
50 P. Thiyagarajan, D. J. Chaiko and R. P. Hjelm, *Macromolecules*, 1995, **28**, 7730–7736.
51 N. L. Abbott, D. Blankschtein and T. A. Hatton, *Macromolecules*, 1992, **25**, 3932–3941.
52 C. Branca, A. Faraone, S. Magazu, G. Maisano, P. Migliardo and V. Villari, *J. Mol. Liq.*, 2000, **87**, 21–68.
53 P. G. DeGennes, *Scaling Concepts in Polymer Physics*, Ithaca, NY: Cornell Univ. Press, 1979.
54 A. R. Rennie, R. J. Crawford, E. M. Lee, R. K. Thomas, T. L. Crowley, S. Roberts, M. S. Qureshi and R. W. Richards, *Macromolecules*, 1989, **22**, 3466–3475.
55 J. A. Henderson, R. W. Richards, J. Penfold, R. K. Thomas and J. R. Lu, *Macromolecules*, 1993, **26**, 4591–4600.
56 J. R. Lu, T. J. Su, R. K. Thomas, J. Penfold and R. W. Richards, *Polymer*, 1996, **37**, 109–114.
57 M. W. Kim and B. H. Cao, *Europhys. Lett.*, 1993, **24**, 229–234.
58 B. H. Cao and M. W. Kim, *Faraday Discuss.*, 1994, **98**, 245–252.
59 M. W. Kim, *Colloids Surf., A*, 1997, **128**, 145–154.
60 M. Darvas, T. Gilanyi and P. Jedlovszky, *J. Phys. Chem. B*, 2010, **114**, 10995–11001.
61 D. J. Kuzmenka and S. Granick, *Polym. Commun.*, 1987, **29**, 64.
62 D. J. Kuzmenka and S. Granick, *Macromolecules*, 1988, **21**, 779–782.
63 B. B. Sauer and H. Yu, *Macromolecules*, 1989, **22**, 786–791.
64 T. Gilanyi, I. Varga, M. Gilanyi and R. Meszaros, *J. Colloid Interface Sci.*, 2006, **301**, 428–435.
65 R. L. Shuler and W. A. Zisman, *J. Phys. Chem.*, 1970, **74**, 1523–&.
66 D. J. Kuzmenka and S. Granick, *Polym. Commun.*, 1988, **29**, 64–66.
67 M. Kawaguchi, S. Komatsu, M. Matsuzumi and A. Takahashi, *J. Colloid Interface Sci.*, 1984, **102**, 356–360.
68 A. F. Miller, M. R. Wilson, M. J. Cook and R. W. Richards, *Mol. Phys.*, 2003, **101**, 1131–1138.
69 P. M. Anderson and M. R. Wilson, *J. Chem. Phys.*, 2004, **121**, 8503–8510.

Acknowledgments

The authors thank the Royal Thai Government Scholarship for providing funding for a Ph.D. studentship for KP, and Durham University for providing computer time on its high performance computer parallel supercomputer - Hamilton. The authors would like to thank one of the referees for bringing to our attention the possible influences of potasium ions and polydispersity on experimental results of PEG/water systems.

Graphical Abstract

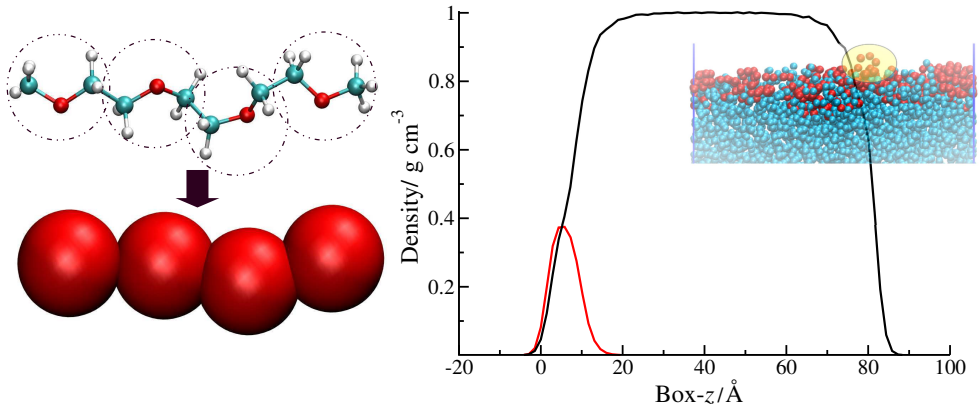

A coarse-grained model for polyethylene glycol (PEG) in water and at a water/air interface.